A Bio-Inspired Micro Air Vehicle and the Experimental Setup for Aerodynamic Testing

W.-L. Chan*, H.-Y. Chen, C.-L. Chin, and C.-H. Huang
National Cheng Kung University, No. 1, University Road, Tainan 70101, Taiwan

ABSTRACT

This paper presents the design, construction, and preliminary testing of the bio-inspired micro air vehicle (MAV), CKopter-1. The MAV features a stable design with dual pairs of wings and a tail for flight control, achieving thrust via the clap-and-fling effect. Detailed geometrical parameters and weight distribution of the CKopter-1 are provided. An experimental setup combining a fan array wind system, a six-axis robotic arm, and a load cell was developed to further investigate the MAV's aerodynamic performance. Calibration of the fan array wind system and initial force measurements were conducted. The results highlighted the MAV's trimmed flight condition, although discrepancies between flight and fan array tests were noted. The findings indicate that while the current setup provides a systematic approach to assessing the aerodynamic performance of the CKopter-1, further refinements are necessary. The preliminary results pave the way for developing a comprehensive aerodynamic model for the MAV.

1 INTRODUCTION

Micro air vehicles (MAVs) have increasingly captivated researchers in recent years, driven by their potential in surveillance, environmental monitoring, and search-and-rescue operations, all while maintaining a compact form factor. Among the diverse MAV designs, bio-inspired MAVs stand out for their efficiency and maneuverability, drawing inspiration from the flight mechanics of birds and insects. Early efforts on bio-inspired flight focused on comprehending the dynamics of unsteady aerodynamics employed by flapping wings [1, 2, 3, 4, 5, 6, 7], with subsequent research transitioning towards applying this aerodynamic understanding to the development of functional flying prototypes. Over the past decade, the design and construction of bio-inspired MAVs have experienced exponential growth. While it is impossible to mention every single bio-inspired MAV prototype, several pioneering projects have stood the test of time and remained active for many years, such as the DelFly [8, 9], RoboBee [10, 11], KUBeetle [12, 13], and Colibri [14, 15]. Among these, DelFly has progressed from inherently stable prototypes to highly agile tailless prototypes [16]. Similarly, the NUS Flowerfly project [17, 18] has undergone a comparable transition.

While control and stability have been achieved in these prototypes, there remains a notable absence of comprehensive studies on the flight characteristics of these flying machines. Consequently, the design of bio-inspired MAVs often relies heavily on trial-and-error processes. Many prototypes are initially constructed without specific performance criteria in mind. A deeper understanding of flight characteristics would enable the integration of stability, controllability, and maneuverability considerations directly into the design process, facilitating the development of MAVs that meet defined requirements.

Over the years, attempts have been made to develop flight dynamic models of bio-inspired flying machines. For insect-inspired or hummingbird-like prototypes, some models are based on empirical aerodynamic models or computational fluid dynamics (CFD) simulations [19, 20, 21]. Due to the significant complexity of such studies, only a handful have included data measurement from actual prototypes [22, 23, 24]. Consequently, efforts to generalize the flight characteristics of these types of flying machines remain scarce.

In light of the discussion above, the primary objectives of this study are to design and fabricate a bio-inspired MAV as a testing platform to explore the potential for agile flight inherent in bio-inspired solutions, and to construct an experimental setup that systematically studies the aerodynamics and flight dynamics characteristics of such flying machines. This paper outlines the preliminary work towards achieving that goal.

This paper is structured as follows: Section 2 details the design and construction of the CKopter-1, including its flapping mechanism and wing fabrication. Section 3 describes the experimental setup and calibration process. Section 4 presents preliminary test results, and Section 5 concludes with a discussion on future work and potential improvements.

2 THE BIO-INSPIRED MAV

The bio-inspired MAV prototype, named the 'CKopter-1' is as shown in Figure 1. It is an inherently stable design with two pair of wings and a tail for stabilization and flight control, much like many other inherently stable flapping wing MAVs designed and flown around the World. The pairs of wings produces thrust by utilizing the clap-and-fling effect. Flight maneuvering is achieved by utilizing the elevator and rudder

*Email address(es): woeileong_chan@gs.ncku.edu.tw

for pitch and yaw controls respectively. The relative position of the center of gravity (CG) and the aerodynamic centers (ACs) as show in Figure 2 makes the prototype very stable in the roll direction, hence roll control is not needed.

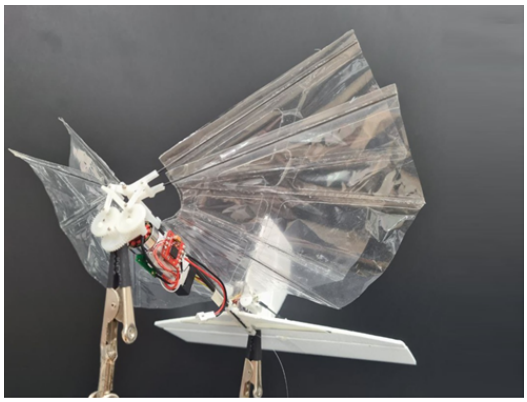

Figure 1: The bio-inspired MAV, CKopter-1.

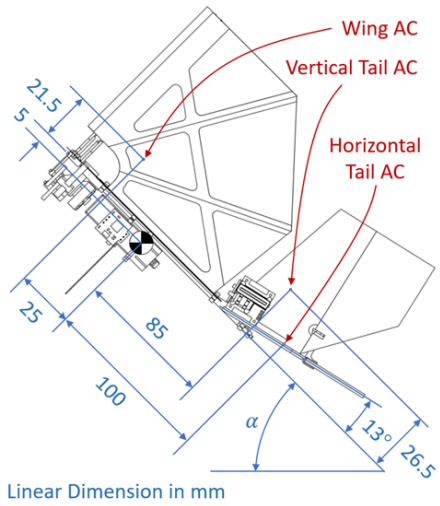

Figure 2: The estimated center of gravity and the aerodynamic centers.

The ACs shown in Figure 2 were estimated based on the geometrical parameters shown in Table 1. Since the prototype has four wings, it must be emphasized that the one-sided area of the wing is for one wing from root to tip. The data for the mean aerodynamic chord (MAC) was calculated using Equation 1, where S, $b/2$, c, and y stand for one-sided area, root-to-tip span, chord length, and distance in the span direction.

$$\bar{\bar{c}} = \frac{1}{S}\int_0^{\frac{b}{2}} c(y)^2\, dy \tag{1}$$

Based on the geometrical parameters, the tail volumes are 0.3327 and 0.2610 for the vertical and horizontal tails, respectively. The tail volumes were calculated using Equation 2 and Equation 3, where the subscripts v, h and w represent the vertical tail, horizontal tail, and the wing. In this context, the wing area S_w refers to the total area of a pair of wings from tip-to-tip. The symbol l, commonly referred as the arm length, denotes the longitudinal distance between the center of gravity (CG) and the AC of the respective tail surface.

	One-Sided Area (mm^2)	Root-to-Tip Span (mm)	MAC (mm)
Wing	8000	100	89.48
Horizontal Tail	4166	75	57.56
Vertical Tail	3157	63	50.67

Table 1: Geometrical parameters of the wing and tail.

$$\overline{V}_v = \frac{S_v l_v}{S_w b_w} \tag{2}$$

$$\overline{V}_h = \frac{S_h l_h}{S_w \bar{\bar{c}}_w} \tag{3}$$

The prototype has a total weight of 17.25gf. Figure 3 illustrates the weight distribution. Most of the weight comes from the 1 cell (1S) 130mAh lithium polymer (LiPo) battery, the two linear servos (LSM1300), the brushless motor (OP03X 20000Kv), the wings, and the flapping mechanism. The structural components, made primarily of 1.4mm $\times$ 1.4mm square carbon fiber rod, 1.5mm foam board, and Polyoxymethylene (POM), constitutes only 6% of the total mass. The lightweight avionics comprise the electronic speed controller (MX-3A) and the remote control receiver (DelTang 2.4GHz receiver).

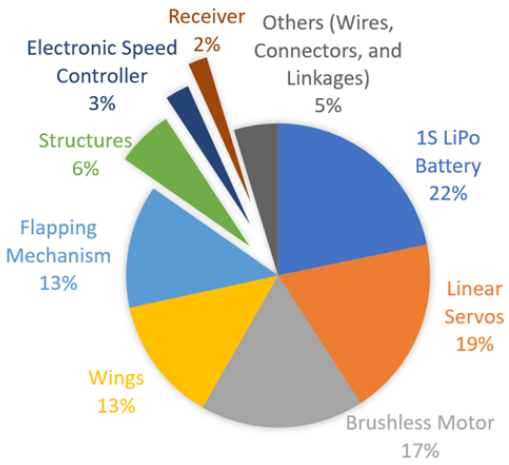

Figure 3: Weight distribution of CKopter-1.

2.1 *Flapping Mechanism*

The CKopter-1 was designed to be a reliable platform for further investigation into bio-inspired flight dynamics. Therefore, a relatively conventional mechanism was chosen: a double crank-rocker mechanism, with each crank-rocker driving a pair of wings as shown in Figure 4. The 25.4:1 gear reduction ratio mechanism was adapted from an off-the-shelf mechanism rather than being proprietary. While the base structure and gears of the original mechanism were retained, significant modifications were made to the crank-rocker to enable clap-and-fling motions on the sides and top within a single flapping cycle as illustrated in Figure 5. These modified components were made from POM using an in-house computer numerical control (CNC) milling machine. The modification also allows each wing to have significantly larger stroke angle, which is 55° per wing.

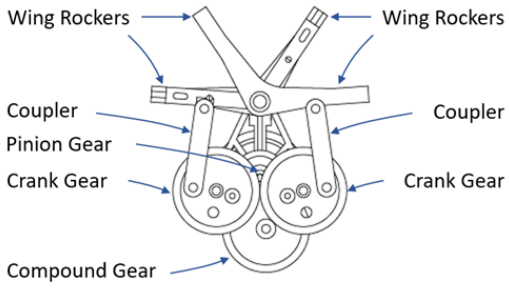

Figure 4: Flapping mechanism.

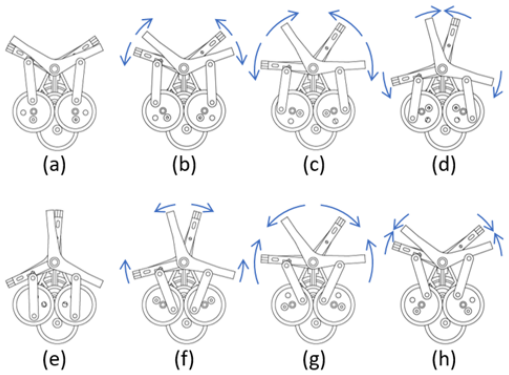

Figure 5: The flapping cycle.

2.2 *Wings*

The wing has a root chord of approximately 90mm and a tip chord of 50mm, with tapering starting at half the root-to-tip span. A 5° angle was added at the wing root, as depicted in Figure 6, to encourage wing rotation through wing twist deformation during flapping. It's worth noting that one side of the wing has a shorter chord than the other, differing by 3mm to accommodate the wing installation on the wing rocker. The wing membrane is made of 8μm transparent biaxially oriented polyethylene terephthalate (BoPET) film. The stiffeners, wing root, and leading edge are made of rounded carbon rods with diameters of 0.3mm, 0.6mm, and 0.8mm, respectively. These carbon rods were attached to the BoPET film using polyvinyl acetate-based adhesive, with transparent polyvinyl chloride (PVC) stickers added on top of the rods to reinforce the adhesion, as illustrated in Figure 7.

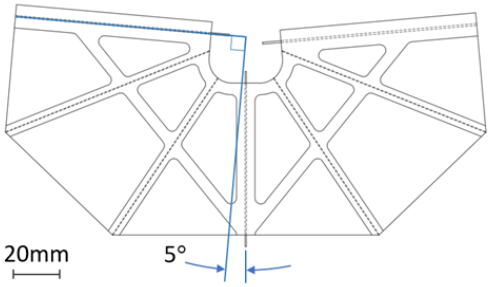

Figure 6: The working sequence of the flapping mechanism.

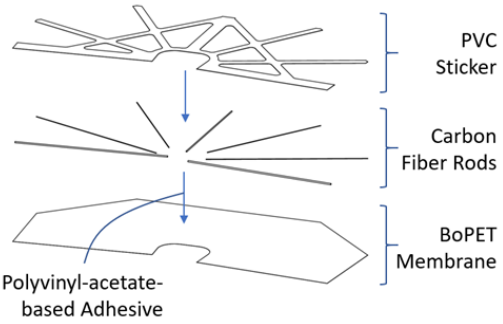

Figure 7: Fabrication of the wings.

2.3 *Trimmed Flight*

Remote piloted flight tests were conducted to assess the flight characteristics of CKopter-1, particularly to understand the trimming of control surfaces and to estimate the trim condition of the flight. Figure 8 shows a composite image extracted from high-speed video recording of a cruise flight. The trim condition was estimated using the video, revealing a cruise speed of approximately 1m/s and a flight incident angle (α) of about 43°. Furthermore, the flapping frequency was estimated to be 15.6Hz. It must be emphasized that achieving trimmed cruise flight in a confined space was extremely challenging. The estimated trim condition helped narrow down the testing range for the aerodynamic testing discussed in the subsequent section.

3 THE EXPERIMENTAL SETUP

As illustrated in Figure 9, the experimental setup for the aerodynamic test consists of a robotic arm holding a load cell

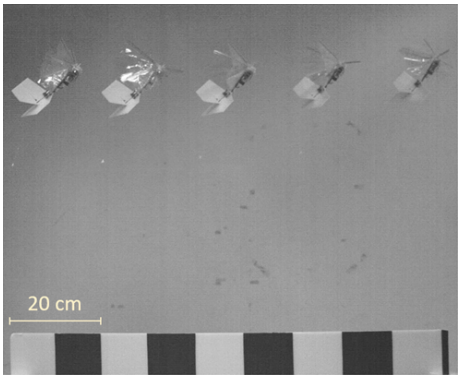

Figure 8: Flight test to estimate the trimmed condition of the prototype.

with the prototype attached. Incoming airflow is provided by a 5×5 fan array wind system. The robotic arm has six degrees of freedom (DoF), allowing users to control both transitional and rotational motion of the end effector. Specifically, the Xarm6 robotic arm is utilized, boasting a reach of 700mm, a travel speed of 1m/s, a rotational speed of 180°/s, and a maximum payload capacity of 5kg. The load cell used is the ATI Mini40, capable of measuring 3-axis forces and 3-axis torque. Such a setup promises future potential for dynamic testing.

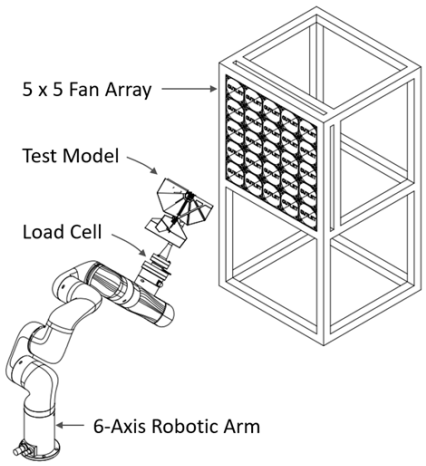

Figure 9: The experimental setup.

3.1 Fan Array Wind System

The design of the experimental setup was inspired by similar work using fan array systems [25]. The fan array wind system was assembled in-house using 25 high-performance cooling fans (Delta GFC0812DW-SM0113Y). Each fan features two counter-rotating blades and operates at 12V direct current (DC). With a maximum power consumption rated at 119.09W per fan and a maximum airflow of 5.015m^3/minute, the theoretical maximum wind speed is approximately 13m/s given the fan frontal area of 80×80mm. However, if all 25 fans were to run at maximum speed, they would collectively draw close to 3000W of power. The current DC power supply (GW Instek PSW 30-72) is only capable of supplying a maximum of 720W. Therefore, the current setup is not ready to operate at maximum speed, nor is it necessary to do so, as the trim flight speed of CKopter-1 is significantly below the maximum speed.

The overall system architecture of the fan array is depicted in Figure 10. Each fan is controlled via a pulse-width modulation (PWM) signal through an Arduino UNO, with each Arduino UNO managing five fans. A master Arduino UNO acts as the bridge, receiving user commands from a personal computer (PC) via a universal serial bus (USB) and sending commands to the other Arduinos to control individual fan speeds via the universal asynchronous receiver/transmitter (UART) protocol. All the Arduino codes were developed in-house.

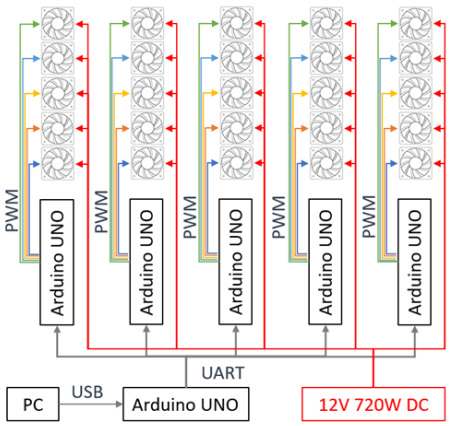

Figure 10: System architecture of the fan array.

The fan array system offers several advantages over traditional wind tunnels. The smaller fans have a faster reaction time, and when combined with independent control, they enable the generation of complex wind fields. The unbounded testing area reduces restrictions, opening up many possibilities for dynamic motion tests. For instance, in our case, we positioned a robotic arm downstream in the testing area. However, the system's downside is the significantly higher turbulence, which makes it less suitable for investigating delicate flow fields, though it may more accurately reflect the turbulent conditions of free flight.

In this study, the robotic arm was used to adjust the flight incident angle (α), as illustrated in Figure 11. The test model's rotational motion was centered on the CG position of the CKopter-1. While this setup was utilized for static testing, it can be extended to dynamic testing, where force and moment data are collected at specific pitch rates.

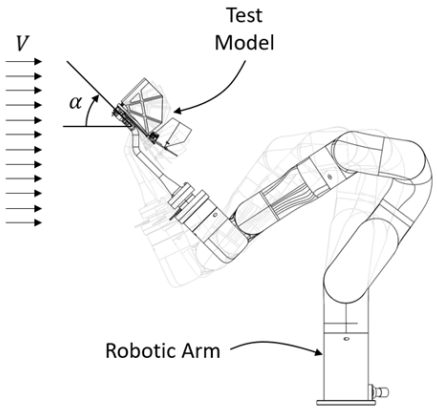

Figure 11: Robotic arm motion to achieve flight incident angle in the experiment.

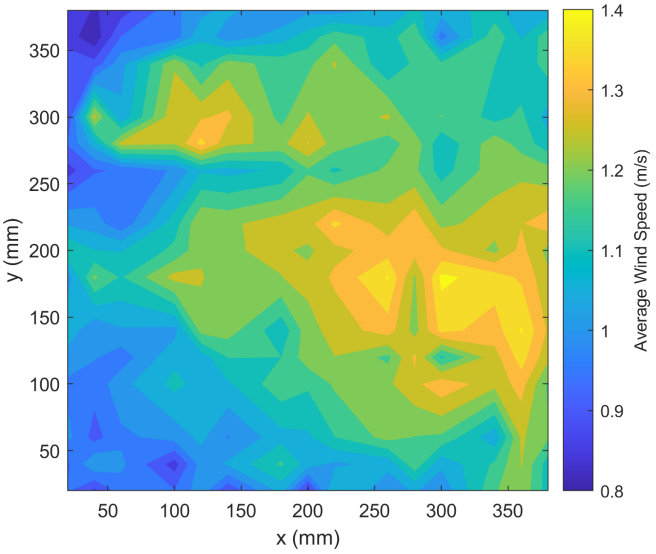

Figure 12: Average wind speed contour of the fan array at minimum speed setting.

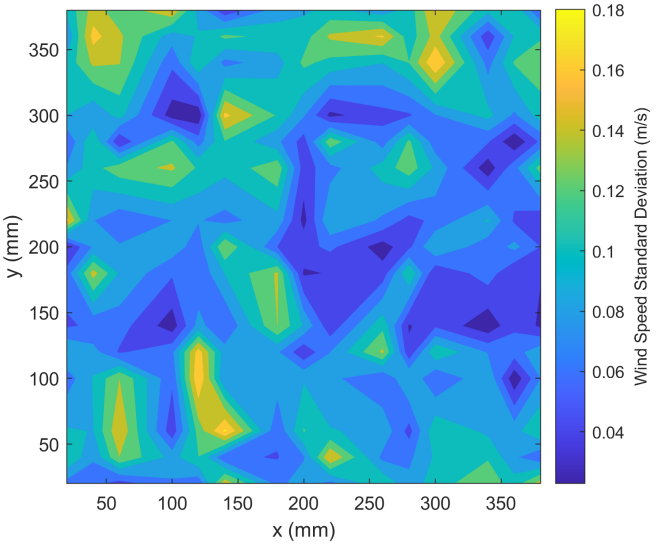

Figure 13: Wind speed standard deviation contour of the fan array at minimum speed setting.

4 CALIBRATION AND PRELIMINARY TEST RESULTS

4.1 *Fan Array Calibration*

The calibration of the fan array was conducted with the robotic arm holding a Benetech GT8911 hot wire anemometer, scanning through the entire 400×400mm area at 20mm intervals using a robotic arm. The target wind speed was approximately 1.1m/s, which corresponds to the estimated cruise speed of CKopter-1. An unforeseen challenge during the calibration process was the lower limit of the PWM signal to which the fans would respond. It was discovered that the fans do not respond to PWM signals lower than a 5% duty cycle. While the fans were intentionally chosen to be overpowered to accommodate higher speed tests in the future, the wind speed was still too high for testing CKopter-1 even at the minimum setting. Consequently, the fan array was positioned 2.8 meters away from the testing model to reduce the average wind speed.

The sampling rate of the wind speed measurement was 1Hz. A total of 10 data points were collected at each measurement point. The wind speed profile is depicted in Figure 12. The average wind speed was 1.14m/s, with the region at the center-right showing a slightly higher wind speed than the rest. Figure 13 depicts the standard deviation of the wind speed measurements. It is evident that the wind speed was very stable, with the highest standard deviation of 0.18m/s occurring at only a few spots. Further work is needed to improve the wind speed distribution for more accurate test results.

4.2 *Preliminary Force Measurement*

Using the attained wind profile, preliminary tests were conducted to determine the trim flight condition using a CKopter-1 test model, which closely resembles the flying prototype. The actual setup is depicted in Figure 14. Tests were conducted at flapping frequencies of 16Hz, with flight incident angles (α) ranging from 40° to 60° at 5° intervals. Tests were performed three times to ensure repeatability.

The cycle-averaged vertical force (positive upward), horizontal force (positive rearward), and pitching moment about the CG (positive pitch-up) are plotted in Figures 15, 16, and 17, respectively. The error bars represent standard deviation. Cycle-averaged force/moment refers to the average measurements over multiple continuous flapping cycles. Both forces exhibit an approximately linear increase with the incident angle. Notably, the horizontal force is the net result of forward thrust and aerodynamic drag. At an incident angle of 56.43°, marked by the red circle in the figures, the forward thrust and

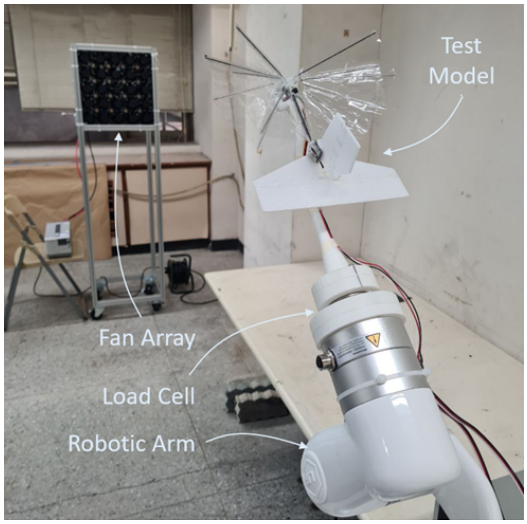

Figure 14: Actual setup in the laboratory.

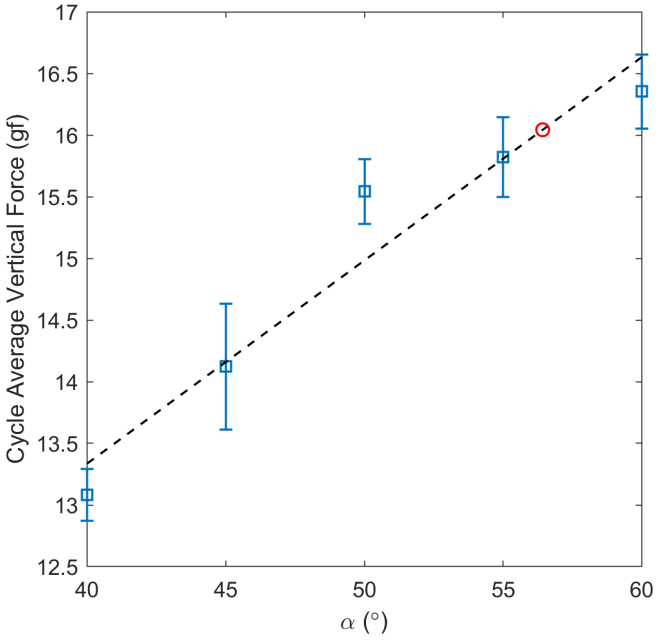

Figure 15: Vertical force at 1.14m/s wind speed and 16Hz flapping frequency.

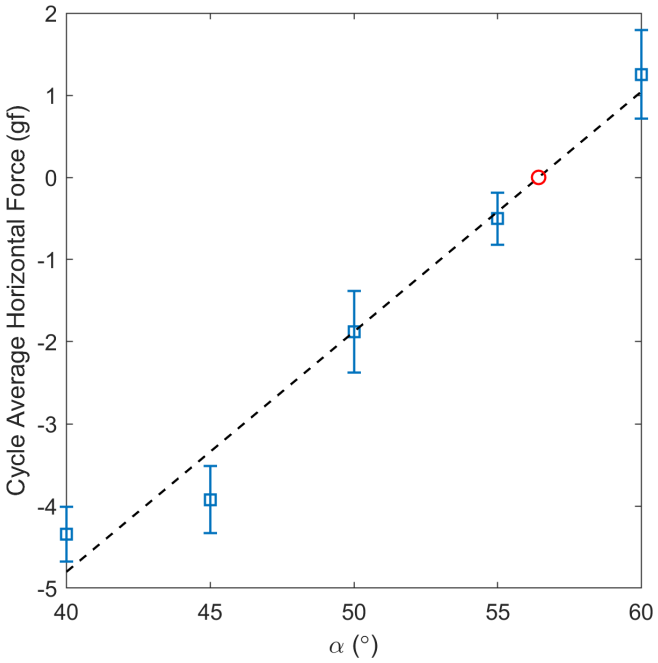

Figure 16: Horizontal force at 1.14m/s wind speed and 16Hz flapping frequency.

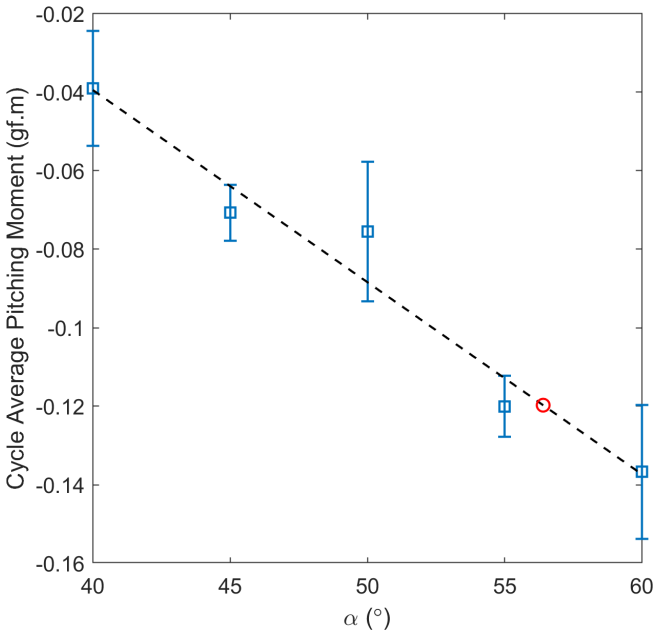

Figure 17: Pitching moment at 1.14m/s wind speed and 16Hz flapping frequency.

aerodynamic drag cancel each other out, indicating a trimmed flight condition where the prototype flies at a constant velocity. However, the vertical force at that point was 16.04 gf, which is less than the total weight of the flying prototype, 17.25 gf, as mentioned in Section 2.

Moreover, while the negative slope of the pitching moment plot confirms the prototype's static stability, it is clear that the pitching moment remains negative within the range of incident angles measured. Further tests are required to identify the trim condition that satisfies the criteria of zero pitching moment, zero horizontal force, and a vertical force of 17.25 gf. It is apparent that the trim condition estimated from the flight test cannot be fully reproduced in the fan array test. Several factors may contribute to this discrepancy, such as increased drag caused by the sting attachment of the test

model, slight differences between the flying prototype and the force measurement test model due to fabrication tolerances, and inaccuracies in pitching moment measurement caused by the load cell's lack of precision and its position far from the CG due to size constraints.

Despite these challenges, the experimental setup provides a systematic way to assess the aerodynamic performance of the CKopter-1 and holds potential for dynamic experiments.

5 CONCLUSION

We have built an inherently stable bio-inspired MAV and performed remote control flight tests to estimate its trim condition. To further understand its aerodynamic performance, we designed and constructed an experimental setup to facilitate dynamic modeling. This setup combines a fan array wind system, a six-axis robotic arm, and a load cell, allowing us to measure the forces and moments acting on the MAV during various orientation. Although more work is needed to perfect the setup, our preliminary results are promising and indicate that a comprehensive aerodynamic model can be developed in the future. Future work includes improvement on the fan array calibration, utilizing smaller and more precise load cells, conduct dynamic test, and possibly incorporating a motion capture system to accurately track the test model's motion.

ACKNOWLEDGEMENTS

This project was supported by the National Science and Technology Council of Taiwan (112-2222-E-006-001-MY3).

REFERENCES

[1] H. Liu, C.P. Ellington, K. Kawachi, C. van den Berg, and A.P. Willmott. A computational fluid dynamic study of hawkmoth hovering. *Journal of Experimental Biology*, 201(4):461–477, 1998.

[2] M.H. Dickinson, F.O. Lehmann, and S.P. Sane. Wing rotation and the aerodynamic basis of insect flight. *Science*, 284(5422):1954–1960, 1999.

[3] Z.J. Wang. Vortex shedding and frequency selection in flapping flight. *Journal of Fluid Mechanics*, 410:323–341, 2000.

[4] R. Ramamurti and W. Sandberg. A three-dimensional computational study of the aerodynamic mechanisms of insect flight. *Journal of Experimental Biology*, 205(10):1507–1518, 2002.

[5] S.P. Sane. The aerodynamics of insect flight. *Journal of Experimental Biology*, 206(23):4191–4208, 2004.

[6] Z.J. Wang, J.M. Birch, and M.H. Dickinson. Unsteady forces and flows in low reynolds number hovering flight: Two-dimensional computations vs robotic wing experiments. *Journal of Experimental Biology*, 207(3):449–460, 2004.

[7] F.O. Lehmann, S.P. Sane, and M.H. Dickinson. The aerodynamic effects of wing-wing interaction in flapping insect wings. *Journal of Experimental Biology*, 208(16):3075–3092, 2005.

[8] G. de Croon, K.M.E. de Clerq, R. Ruijsink, B. Remes, and C. De Wagter. Design, aerodynamics, and vision-based control of the delfly. *International Journal of Micro Air Vehicles*, 1(2):71–97, 2009.

[9] C. De Wagter, S. Tijmons, B.D.W. Remes, and G.C.H.E. de Croon. Autonomous flight of a 20-gram flapping wing mav with a 4-gram onboard stereo vision system. In *IEEE Conference on Robotics and Automation (ICRA)*, 2014.

[10] K.Y. Ma, P. Chirarattananon, S.B. Fuller, and R.J. Wood. Controlled flight of a biologically inspired insect-scale robot. *Science*, 340(6132):603–607, 2013.

[11] E.F. Helbling, S.B. Fuller, and R.J. Wood. *Altitude estimation and control of an insect-scale robot with an onboard proximity sensor*, pages 57–69. Springer International Publishing, 2018.

[12] H.V. Phan, T. Kang, and H.C. Park. Design and stable flight of a 21g insect-like tailless flapping wing micro air vehicle with angular rates feedback control. *Bioinspiration & Biomimetics*, 12(3), 2017.

[13] H.V. Phan, S. Aurecianus, T. Kang, and H.C. Park. Kubeetle-s: An insect-like, tailless, hover-capable robot that can fly with a low-torque control mechanism. *International Journal of Micro Air Vehicles*, 11(3), 2019.

[14] A. Roshanbin, H. Altartouri, M. Karasek, and A. Preumont. Colibri: A hovering flapping twin-wing robot. *International Journal of Micro Air Vehicles*, 9(4):270–282, 2017.

[15] A. Preumont, H. Wang, S. Kang, K. Wang, and A. Roshanbin. A note on the electromechanical design of a robotic hummingbird. *Actuators*, 10(3), 2021.

[16] M. Karásek, F.T. Muijres, C. De Wagter, B.D.W. Remes, and G.C.H.E. de Croon. A tailless aerial robotic flapper reveals that flies use torque coupling in rapid banked turns. *Science*, 361(6407):1089–1094, 2018.

[17] Q.V. Nguyen, W.L. Chan, and M. Debiasi. Experimental investigation of wing flexibility on force generation of a hovering flapping wing micro air vehicle with double wing clap-and-fling effects. *International Journal of Micro Air Vehicles*, 9(3):187–197, 2017.

[18] Q.V. Nguyen and W.L. Chan. Development and flight performance of a biological-inspired tailless flapping

wing micro air vehicle with wing stroke plane modulation. *Bioinspiration & Biomimetics*, 14(1):016015, 2018.

[19] M. Sun. Insect flight dynamics: stability and control. *Reviews of Modern Physics*, 86:615–646, 2014.

[20] S. Biswal, M. Mignolet, and A.A. Rodriguez. Modeling and control of flapping wing micro aerial vehicles. *Bioinspiration & Biomimetics*, 14(2):026004, 2019.

[21] B. Singh, K.A. Ahmad, M. Murugaiah, N. Yidris, A.A. Basri, and R. Pai. Quasi-steady aerodynamic modeling and dynamic stability of mosquito-inspired flapping wing pico aerial vehicle. *Frontiers in Robotics and AI*, 11, 2024.

[22] F.Y. Hsiao, T.M. Yang, and W.C. Lu. Dynamics of flapping-wing mavs: application to the tamkang golden snitch. *Journal of Applied Science and Engineering*, 15(3):227–238, 2012.

[23] K.M. Kajak, M. Karásek, Q.P. Chu, and G.C.H.E. de Croon. A minimal longitudinal dynamic model of a tailless flapping wing robot for control design. *Bioinspiration & Biomimetics*, 14(4):046008, 2019.

[24] R. McGill, N.-S.P. Hyun, and R.J. Wood. Modeling and control of flapping-wing micro-aerial vehicles with harmonic sinusoids. *IEEE Robotics and Automation Letters*, 7(2):746–753, 2022.

[25] D.A. Olejnik, S. Wang, J. Dupeyroux, S. Stroobants, M. Karasek, C. De Wagter, and G. de Croon. An experimental study of wind resistance and power consumption in mavs with a low-speed multi-fan wind system. In *2022 International Conference on Robotics and Automation (ICRA)*, pages 2989–2994, 2022.